A two-surface plastic model for concrete behaviour

Ludovic Jason, Sabine Durand

A two-surface plastic model for concrete behaviour

Ludovic Jason - Sabine Durand

CEA SACLAY
DM2S / SEMT / LM2S
Bat. 607
91191 Gif sur Yvette Cedex, France
Ludovic.Jason@cea.fr

RÉSUMÉ. *La qualité d'un modèle de comportement est généralement évaluée autour de trois critères : sa capacité à reproduire des comportements élémentaires ou structurels représentatifs (traction, compression, flexion…), l'efficacité de son implémentation (algorithme de résolution, convergence) et la simplicité de calibrage des paramètres qu'il utilise (ou leur signification physique). Un modèle plastique est présenté dans cette contribution. Nécessitant huit coefficients physiquement représentatifs, il se compose de deux surfaces seuil adoucissantes, l'une pour la traction (Rankine), l'autre pour la compression (Drucker-Prager). Après une brève présentation des équations constitutives, la loi est testée avec succès sur des applications élémentaires (traction, compression, essai biaxial) et structurelles (poutre en flexion trois points et cylindre armé chargé en température) afin de valider l'implémentation. Le modèle représente, par sa relative simplicité (numérique et signification physique des paramètres) , un bon compromis pour le comportement du béton, face à d'autres approches, plus élaborées mais aussi plus complexes à mettre en œuvre.*

ABSTRACT. The quality of a mechanical law is generally based on the evaluation of three parameters : its ability to reproduce elementary or structural characteristic behaviours (tension, compression, bending…), the efficiency of the numerical implementation (resolution algorithm or convergence) and the physical significance of its parameters. A plastic model is presented in this contribution. Based on eight coefficients which are physically representative, it is driven by two softening yield surfaces, one for tension (Rankine) and one for compression (Drucker-Prager). After a brief description of the constitutive equations, the model is tested on elementary and structural applications to validate its numerical implementation. It represents a good compromise for classical concrete behaviours, compared to other more refined, but also more complex, approaches.

MOTS-CLÉS : *modèle, béton, plasticité.*

KEYWORDS: *constitutive model, concrete, plasticity*

1. Introduction

Understanding the consequences of a mechanical loading on the behaviour of a concrete specimen or of concrete structures is of great concern, especially when it is related to safety questions. It is the case for high-power French nuclear power plants (1300 and 1450 MWe especially) for which the concrete containment vessel represents the third passive barrier, after the fuel cladding and the containment vessel of the reactor core. That is why, for the last decade, several important civil engineering research and development programs have been launched. These concern the elaboration of new constitutive laws, techniques of modelling and resolution algorithms. The validity of the models and more generally the methodology for non-linear calculations must be obtained by comparing their performances with experimental results (benchmarking (Ghavamian and Delaplace, 2003) for example). The comparisons are generally based on simple tests on small size specimen but also on more complex applications to determine the capacity of the calculations to predict the structural behaviour of more realistic and/or industrially representative cases. The quality of a model is generally estimated from its ability to reproduce elementary and structural characteristic behaviours, like tension, compression or bending. But, two other parameters have also to be taken into account : the efficiency of the numerical implementation (convergence) and the physical significance of the coefficients of the model. It is especially the case for industrial applications for which the numerical cost may be heavy (due to a need in fine meshes) and the knowledge of the material properties is limited (Young modulus, compressive strength…).

When continuum mechanics is considered, elastic damage models or elastic plastic constitutive laws are generally the standard approaches to describe the behaviour of concrete. In the first case, the mechanical effect of the progressive microcracking and strain softening is represented by a set of internal state variables, which acts on the elastic behaviour (decrease of the stiffness) at the macroscopic level (see for example (Simo and Ju, 1987a), (Simo and Ju, 1987b) or (Mazars, 1984)). In plasticity models, softening is directly included in the expression of a plastic yield surface by means of a hardening – softening function generally ((Grassl et al, 2002), (Menetrey and Willam, 1995), or (Crouch and Tahar, 2000)). In particular cases, for which the estimation of the unloading behaviour is of great concern (damage – permeability law for example (Picandet et al, 2001)), coupled approaches can also be considered to simulate both plasticity effects, with the development of irreversible phenomena and damage, with a decrease in the unloading slope ((Oller et al, 1990), (Yazdani and Schreyer, 1990) or (Jason et al, 2006)).

The models that have been previously mentioned generally require the identification of many parameters (from 5 with Mazars' model (1984) to 20 or even more for coupled formulations) whose experimental significance is not totally obvious. The idea is thus to propose in this contribution a formulation as simple as

possible that would be adapted for standard applications, for which a high level of refinement is not necessary (monotonic loading especially) but whose coefficients can be clearly calibrated from standard material properties. A plastic model, with eight coefficients, is thus presented. It is driven by two softening yield surfaces, one for tension (Rankine) and one for compression (Drucker-Prager). Section 2 presents the constitutive equations and especially the evolution of the yield surfaces with the hardening parameters. The law is then applied on three elementary tests, uniaxial tension, compression and biaxial loading (section 3). Finally, the validation ends with a reinforced bending beam and a concrete cylinder subjected to a thermal loading.

2. Model description

The model has been chosen to fulfil two main objectives : to represent the behaviour of concrete in tension and in compression correctly and to use mechanical parameters that have a physical significance. Based on previous works ((Feenstra and de Borst, 1996) for two dimensional problems or (Heinfling, 1998)), the model is developed from plasticity theory. It uses two yield surfaces, one in tension (Rankine) and one in compression (Drucker-Prager) to take into account the dissymmetry of concrete behaviour in uniaxial loading.

The global mechanical strain ε is written as a function of ε^e, ε^p and ε^{th} which are respectively the elastic, plastic and thermal (if needed) strains:

$$\varepsilon = \varepsilon^e + \varepsilon^p + \varepsilon^{th} \quad [1]$$

The elastic strain is related to the total stress by Hooke law :

$$\sigma = C\varepsilon^e \quad [2]$$

where C is the elastic tensor. The thermal strain is written as a function of the thermal dilation coefficient α_{th}:

$$\varepsilon^{th} = \alpha_{th}(T - T_0)I_d \quad [3]$$

with T and T_0 the current and initial temperatures respectively and I_d the identity tensor. Both yield surfaces (in tension and in compression) are expressed in the following form :

$$f(\sigma, \chi) = f^*(\sigma) - \tau(\chi) \quad [4]$$

where χ is the isotropic hardening variable that governs the evolution of the elastic domain (hardening law τ). For each criterion, the evolution of the plastic strain and of the hardening variable follow the standard plasticity theory :

$$\begin{cases} \dot{\varepsilon}^p = \dot{\lambda}\dfrac{\partial f}{\partial \sigma} \\ \dot{\chi} = -\dot{\lambda}\dfrac{\partial f}{\partial \tau} = \dot{\lambda} \end{cases} \quad [5]$$

In compression, a Drucker-Prager yield surface is considered (Drucker and Prager, 1952):

$$f_1(\sigma, \chi_1) = \sqrt{J_2} + \alpha I_1 - \tau_1(\chi_1) \quad [6]$$

with I_1 and J_2 respectively the first stress and the second deviatoric stress invariants. α is a function of the biaxial and uniaxial compressive strengths (respectively named f_b and f_c) :

$$\alpha = \frac{f_b - f_c}{\sqrt{3}(2f_b - f_c)}$$

The hardening – softening law τ_1 is chosen to represent the progressive evolution of the stress – strain curve in uniaxial compression :

$$\tau_1(\chi_1) = \begin{cases} k_0 f_c[1 + (w-1)\dfrac{(\chi_1 - \chi_{1m})^2}{\chi_{1m}^{\ 2}}] & \text{if } \chi_1 < \chi_{1m} \\ k_0 f_c[1 + (w-1)\dfrac{(\chi_1 - \chi_{1m})^2}{(\chi_{1u} - \chi_{1m})^2}] & \text{if } \chi_{1m} \le \chi_1 \le \chi_{1u} \\ k_0 f_c & \text{if } \chi_1 > \chi_{1u} \end{cases} \quad [7]$$

where w, k_0 , χ_{1m} and χ_{1u} are four parameters.

$$\begin{aligned} w &= \frac{\sigma_y}{f_c} \\ k_0 &= \frac{f_b}{\sqrt{3}(2f_b - f_c)} \\ \chi_{1m} &= \frac{\sqrt{3}}{\sqrt{3}\alpha - 1}(\varepsilon_m + \frac{f_c}{E}) \\ \chi_{1u} &= \frac{\sqrt{3}}{\sqrt{3}\alpha - 1}\varepsilon_u \end{aligned} \quad [8]$$

σ_y is the elastic limit in uniaxial compression. E is the Young modulus and ε_m and ε_u are respectively the strain corresponding to the compressive strength and the ultimate strain respectively. Figure 1 illustrates the hardening-softening law. It follows the characteristic concrete behaviour in compression : a hardening part from the elastic limit to the peak position, then a decreasing softening evolution from the peak to the ultimate strain before a zero residual strength.

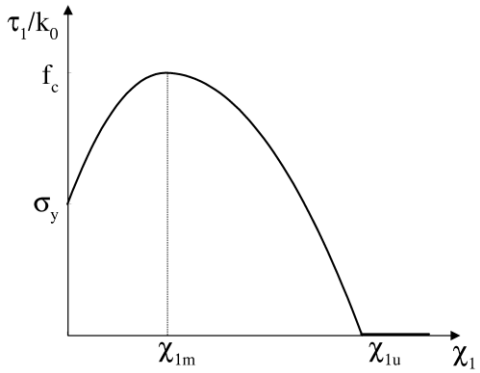

Figure 1. *Hardening – softening law for compression.*

For tension, the yield function is a Rankine surface which can be expressed by :

$$f_2(\sigma, \chi_2) = \sigma_{\max} - \tau_2(\chi_2) \qquad [9]$$

where σ_{max} is the maximum of the principal stresses.

The softening behaviour is driven by the exponential law τ_2 :

$$\tau_2(\chi_2) = f_t \exp(-\frac{\chi_2}{\chi_{2u}}) \qquad [10]$$

with f_t the tensile strength. χ_{2u} is a model parameter, function of the fracture energy G_f and of a characteristic length h to avoid a dependency of the dissipated fracture energy on the mesh (Heinfling, 1998).

$$\chi_{2u} = \frac{G_f}{h.f_t} \frac{1}{1-\exp(-1)} \qquad [11]$$

h is representative of the finite element size and takes the expression ((Rots, 1988) for bi-dimensional problems):

$$\begin{aligned} h &= \sqrt{A_e} \quad \text{for 2D problems} \\ h &= \sqrt[3]{V_e} \quad \text{for 3D problems} \end{aligned} \qquad [12]$$

where A_e and V_e are the surface or the volume of the finite element respectively. More complex expressions (especially for non regular meshes) exist (Millard, 1996) but will not be considered in this contribution.

The tensile softening law is represented in figure 2. The behaviour is elastic before the tensile strength (no hardening domain) then softening appears until a zero residual strength asymptote.

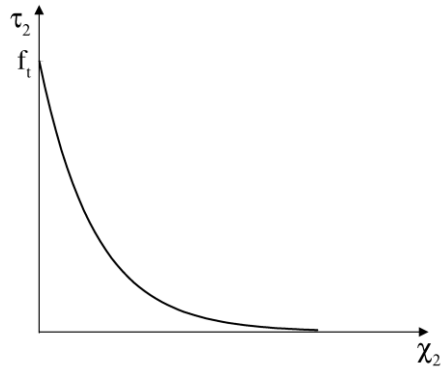

Figure 2. *Softening function for tensile behaviour.*

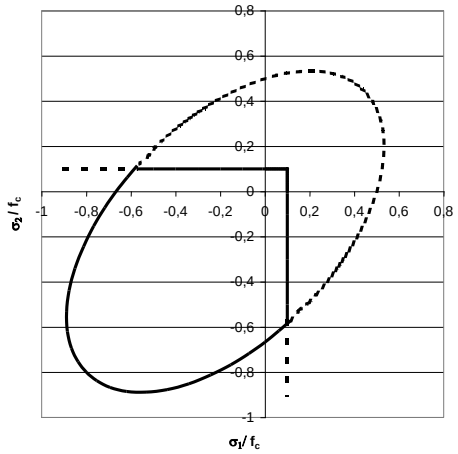

Figure 3. *Elastic yield surface for biaxial loading (dashed lines correspond to the prolongation of Drucker-Prager and Rankine surfaces).*

The model is implemented in the finite element code Cast3M (2006) using a standard return mapping algorithm (Ortiz and Simo, 1986). Figure 3 illustrates the two elastic yield surfaces for biaxial loading ($\sigma_3 = 0$). As expected, for tensile dominant loading, the Rankine surface is the first one to be reached, while for compressive dominant solicitations, it is the Drucker-Prager function which is the first to be activated. Table 1 summarizes the parameters that need to be identified. They are all based on physical material properties and can be obtained from standard material tests, except the biaxial compressive strength and the characteristic length. *h*

is automatically computed by the finite element code, while for the biaxial compressive strength which requires a non standard experiment, default values for $\frac{f_b}{f_c}$ ranging from 1.1 to 1.2 are generally agreed in the literature (Ulm, 1996 for example).

Uniaxial compression				Unaixial tension		Biaxial loading
Elastic limit (Pa)	Compressive strength (Pa)	Strain at peak	Ultimate strain	Tensile strength (Pa)	Fracture energy (N/m)	Biaxial compressive strength (Pa)

Table 1. *Coefficients of the plastic model. The characteristic length h is automatically computed by the code from the type of the finite element.*

It is to be noted that only characteristic experimental points are needed, like compressive strength or fracture energy, contrary to other models for which the total stress – strain curve is necessary to calibrate every parameter (for example (Mazars, 1984) or (Jason et al, 2006) among others). Hence, one concrete material corresponds to a unique set of parameters. It is one of the strong point of the chosen constitutive law.

3. Elementary validation

The model is going to be validated on three elementary applications : uniaxial compression, uniaxial tension and biaxial loading (failure surfaces). The aim is to evaluate the ability of the constitutive law to reproduce standard loadings.

3.1. *Uniaxial tension*

The numerical response of the plastic constitutive law is first compared with experiment from (Gopalaratnam and Shah 1985). The model parameters are shown in Table 2 (ν stands for the Poisson ratio). They are based on a numerical calibration to fit the experimental results. Figure 4 gives the axial stress – strain curve. The model is able to reproduce the peak position and the evolution of the softening part until a zero residual stress. It is thus adapted for uniaxial test simulation and only requires the knowledge of basic material properties (in uniaxial tension, only f_t and G_f are necessary for the calibration)

E (GPa)	ν	σ_y (MPa)	f_c (MPa)	ε_m	ε_u	f_t (MPa)	G_f (N/m)	f_b (MPa)
31.25	0.2	20	35	0.002	0.008	3.5	250	40.6

Table 2. *Model parameters for uniaxial tensile test.*

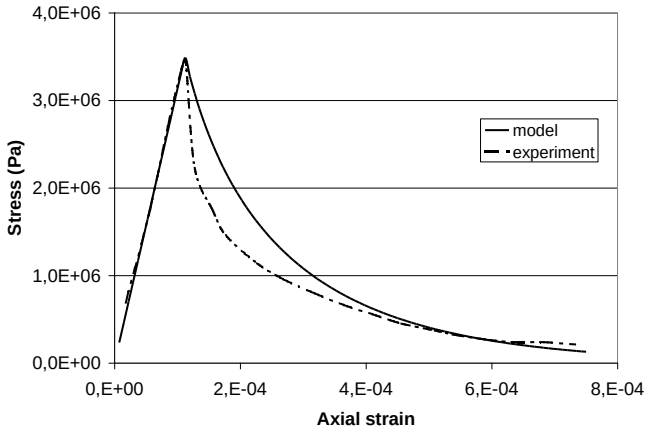

Figure 4. *Uniaxial tensile test. Comparison between simulation and experiment from (Gopalaratnam and Shah, 1985).*

3.2. *Uniaxial compression*

Cyclic compression is the second elementary test used to highlight the interest of the model. Experimental results are taken from (Sinha et al, 1964). Figure 5 illustrates the numerical response for both axial and volumetric strains. The coefficients chosen for this simulation are reported in Table 3. They are different from those in section 3.1. because the tested concrete is different too. The model is able to reproduce the monotonic behaviour (elasticity, hardening and softening). The peak position and the post peak evolution are correctly simulated especially. Concerning the unloading, it is totally misevaluated as it is elastic. The loss in rigidity is not taken into account. If we consider the volumetric response, the evolution from a contractant behaviour to a dilatant one (change in the sign of the volumetric strains) is modelled, as observed experimentally (Sfer et al, 2002).

E (GPa)	ν	σ_y (MPa)	f_c (MPa)	ε_m	ε_u	f_t (MPa)	G_f (N/m)	f_b (MPa)
20.74	0.2	20	27	0.0026	0.008	2.8	250	31.3

Table 3. *Parameters of the plastic model for the uniaxial compressive loading.*

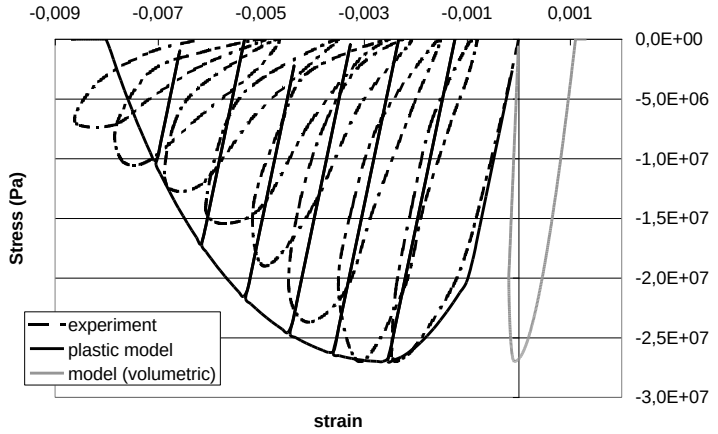

Figure 5. *Uniaxial compression. Comparison between experiment (from (Sinha et al, 1964)) and the plastic model.*

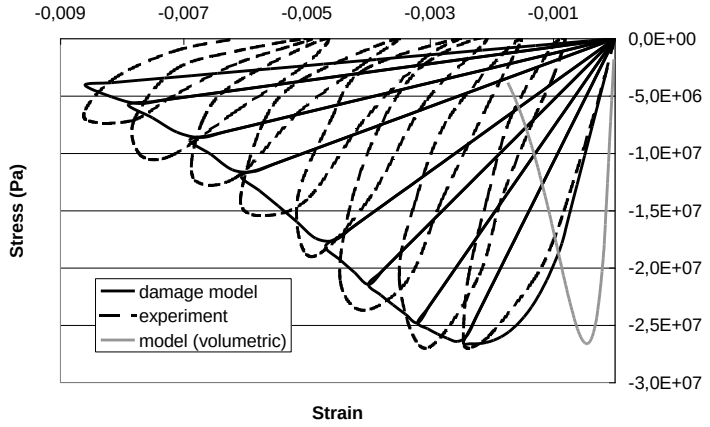

Figure 6. *Uniaxial compression. Comparison between experiment (from (Sinha et al, 1964)) and the damage model (Mazars, 1984).*

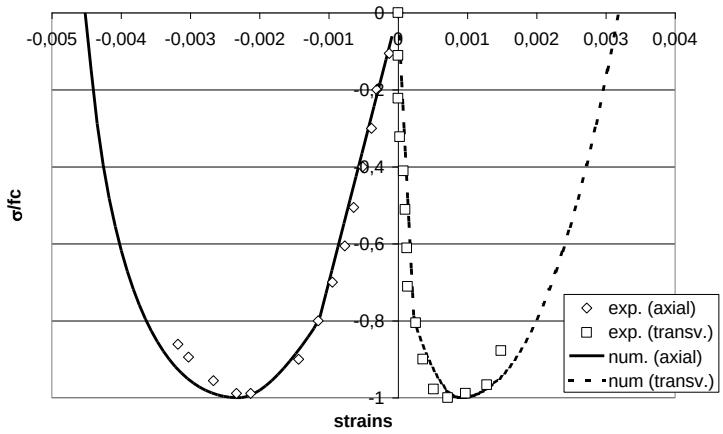

Figure 7. *Monotonic compression. Comparison between experiment (Kupfer et al, 1969) and the plastic model for both axial and transversal responses.*

The response is compared with the simulation using the isotropic damage model developed in its original form by Mazars (1984) and which is generally chosen for its simplicity (figure 6). The monotonic behaviour is also correctly simulated. The unloading behaviour is misevaluated too because no irreversible phenomena are considered (overestimation of the unloading slopes). The volumetric strains keep negative and the change from a contractant behaviour to a dilatant one is not reproduced. As a conclusion, with the same level of simplicity, and with numerical parameters that are directly calibrated from standard material properties, the plastic model enables to capture more information than the isotropic damage model if only monotonic evolution is needed.

Figure 7 shows the simulation of a uniaxial compressive loading for both axial and transversal strains, to provide an entire quantitative comparison. Due to the introduction of plasticity, the constitutive law is able to reproduce the experimental results. It is to be noted that the simulation of the volumetric behaviour may be of great interest, first for mechanical problems, but also for transfer considerations for which concrete permeability can be related to the change in the volumetric response (Sugiyama et al, 1996).

3.3. Biaxial failure surfaces

The failure surfaces for biaxial loading (respectively for $\chi_1 = \chi_{1m}$ for Drucker Prager surface and $\chi_2 = 0^+$ for Rankine criterion) are compared with the experimental data from (Lee et al, 2004) for two different types of concrete (figure 8). In both

cases, $\frac{f_b}{f_c} = 1.2$ and $\frac{f_t}{f_c} = 0.1$ for the numerical computations. The assumed yield contour closely matches experimental results, as already mentioned by (Feenstra and De Borst, 1995) from the experimental results from (Kupfer and Gerstle, 1973). The plastic model is thus able to represent the maximum of the stress during biaxial loading, simply from the knowledge of the ratio between the uniaxial compressive strength and the biaxial compressive and uniaxial tensile strengths respectively. Nevertheless, it is to be noted that the choice for a Rankine yield surface is responsible for a slight overestimation of the mechanical resistance when tensile – compressive biaxial loading are considered.

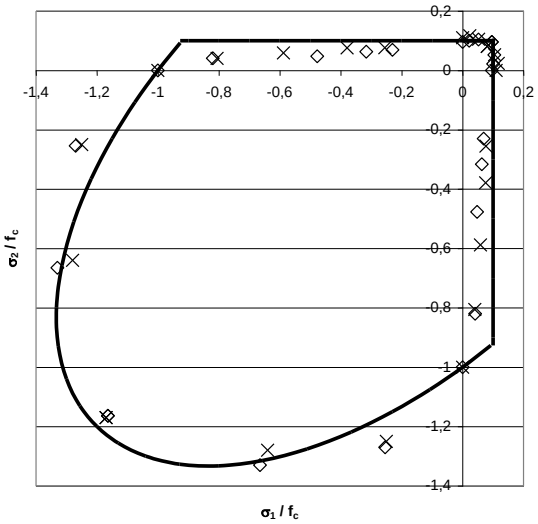

Figure 8. *Biaxial strength envelops for two different types of concrete under biaxial stress. Comparison between the plastic model (black line) and the experiment from (Lee et al, 2004) (discrete points).*

4. Structural validation

After elementary applications, for which the distribution of the internal variables, stresses and strains are homogeneous, the following step is structural tests. In the next part, a reinforced bending beam will be considered before a concrete hollow cylinder subjected to a thermal loading.

4.1. *Three point bending beam*

The first structural application, extracted from benchmarks proposed by EDF (Ghavamian and Delaplace, 2003), is a 3D computation of a reinforced concrete beam. The geometry and the load system are presented in figure 9. Figure 10 depicts the steel distribution. The aim of this test is to evaluate the three dimensional performance of the model. Despite the amount of similar cases that can be found in the literature, this particular test has been chosen because numerical comparisons with models of various complexity (plasticity, isotropic or orthotropic damage …) are already available (figure 11).

Following the requirements of the benchmark, the steel bars are modelled with a Von Mises plasticity law (linear hardening) using the imposed parameters E = 200 GPa (Young modulus), ν = 0 (Poisson ratio), σ_e = 400 MPa (yield stress), E_T = 3245 MPa (plastic tangent stiffness). The steel – concrete interface is assumed to be perfect. Only one fourth of the beam is meshed.

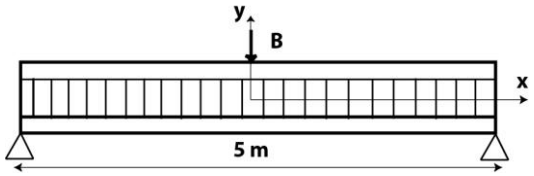

Figure 9. *Geometry of three point bending beam.*

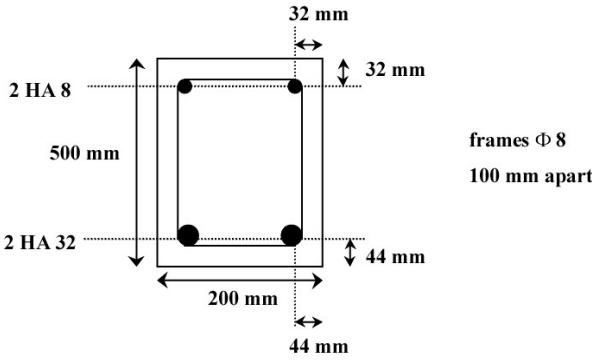

Figure 10. *Steel distribution in the bending beam.*

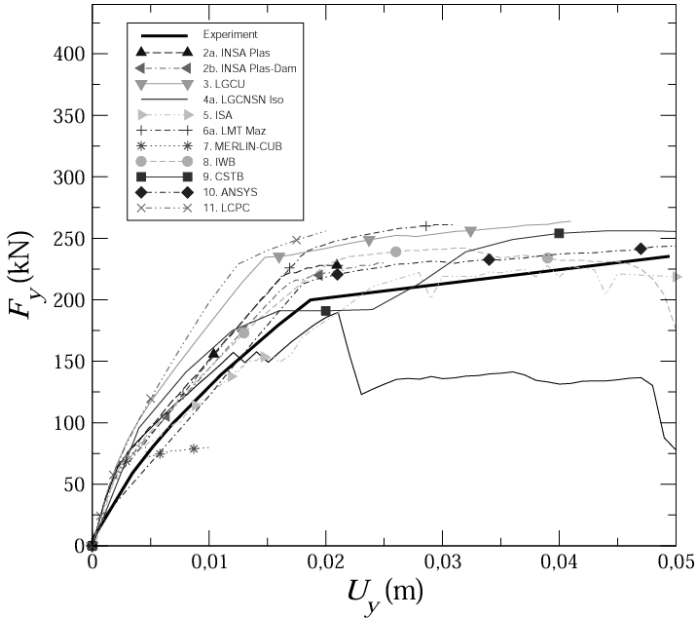

Figure 11. *Benchmark results for the three point bending beam (see (Ghavamian and Delaplace, 2003) for further details).*

E (GPa)	ν	σ_y (MPa)	f_c (MPa)	ε_m	ε_u	f_t (MPa)	G_f (N/m)	f_b (MPa)
37.2	0.2	20	35	0.002	0.007	3.5	400	40.6

Table 4. *Parameters of the plastic model for the three point bending beam.*

Numerical difficulties may appear due to loading conditions on the support and at mid – span loading point. That is why, following the recommendations provided in (Ghavamian and Delaplace, 2003), at the support, a linear elastic behaviour is supposed on the entire cross section of the beam over a length covering one element along the beam axis. At mid span, a vertical uniform displacement is applied over the entire cross section to follow the loading condition. Figure 12 provides the numerical load – deflection curve and a comparison with the experiment, using the parameters given in table 4 and chosen from (Ghavamian and Delaplace, 2003). The results show qualitative similarities. The model exhibits the major characteristics of the beam behaviour : elastic response, first cracking with change in stiffness, tensile reinforcement yielding associated to a ductile plateau and finally some numerical behaviour which may be qualified as the collapse of the structure (decrease of the

force at the end of the computation). Similar evolution was observed with the isotropic damage model developed by Mazars (1984) (Jason et al, 2004). If the results are compared with the benchmark calculations, it can be seen that the plastic model provides an appropriate behaviour, with a limited number of parameters. The overestimation of the force that can be noticed in figure 12 is also noticed for the other constitutive laws. Tailhan et al (2003) explain that if some uncertainties on the experimental parameters (position of the reinforcement, yields stresses for concrete and steel) are taken into account, a change in the ultimate force of the beam from 190 kN to 250 kN (in the range of the simulated results) can be obtained. It could be one of the reasons of the differences observed between experiment and simulation..

Figure 13 presents the distribution of the tensile hardening variable χ_2 at different loading steps. The mechanical degradation is first localised along the surface of symmetry at mid-span. Then a more homogenised zone appears for high level of vertical displacement. If we consider the compressive hardening variable χ_1, it develops at the support point at the end of the computation (not represented here).

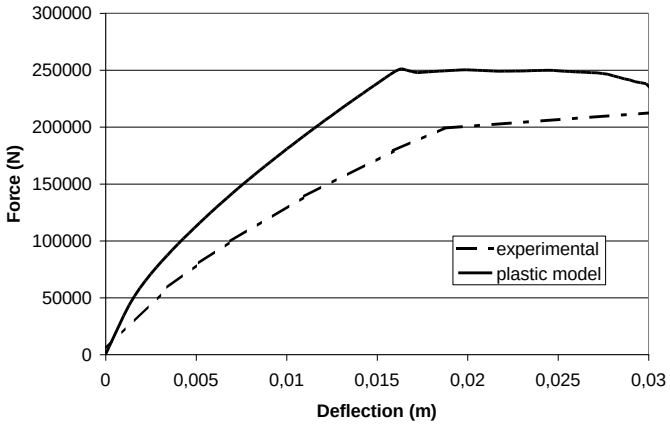

Figure 12. *Load – deflection curve for the three point bending beam.*

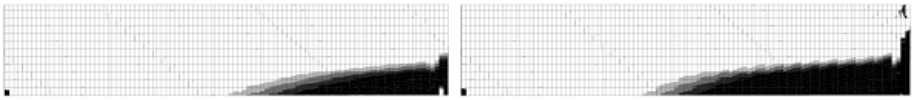

Figure 13. *Tensile hardening variable distribution for three point bending beam for two steps of the computation (black zones are the most damaged ones). Only one fourth of the beam is represented.*

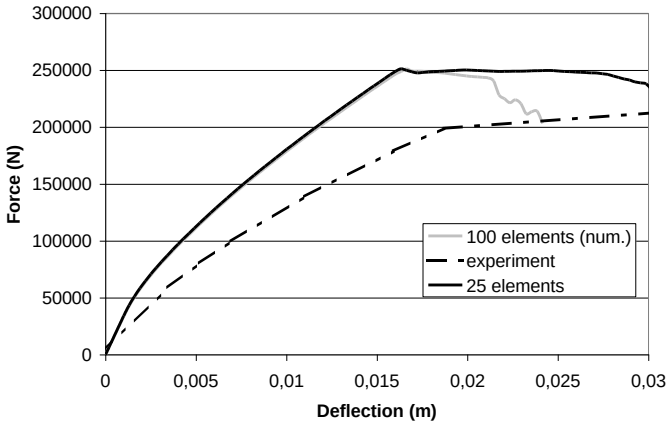

Figure 14. *Load deflections curves for two different meshes (100 and 25 elements in the transversal section).*

To evaluate the mesh influence, figure 14 presents the force – deflection curve for two densities (respectively 25 and 100 elements in the transversal section). The characteristic length seems to play its role during the first steps of the calculation (beginning of the mechanical degradation and tensile yielding). The two responses are indeed exactly similar, until the collapse of the beam, with a high level of internal variables. At the end of the computation, the internal variable indeed localises near the left support (figure 13) with a value higher for the fine mesh than for the coarse one. This localisation problem triggers the end of the computation and explains the differences (and especially the decrease in the force) observed on the force – displacement curve. Nevertheless, the same three evolutions (elasticity, cracking and yielding) are represented with both meshes.

As a conclusion, for three point bending beams, the plastic model is able to reproduce the global behaviour of the structure and especially the successive steps in the mechanical degradation. For local description, the internal tensile variable first localises then propagates into a more homogenised zone. Once again, from the knowledge of standard material properties, and if no refined results is needed (crack pattern distribution for example which is not totally reproduced), the law represents an appropriate tool.

4.2 *Hollow cylinder subjected to thermal loading*

The last application has been designed at the Atomic Energy Commission (Ranc et al, 2003) for the conception of nuclear waste storage structures. It is a reinforced

hollow concrete cylinder with an inner and outer diameter of 1 and 2.2 meters respectively and a height of 3 m (figure 15). The structure is heated from the inside volume, using hollow aluminium cylinders equipped by resistors and is subjected to the loading path depicted in figure 16. The mock-up is laid on a 60 mm thick wood plate and its top is recovered with a 200 mm thick insulator layer and a 30 mm thick wood layer. The aim is to evaluate the behaviour of the material when high temperatures are applied.

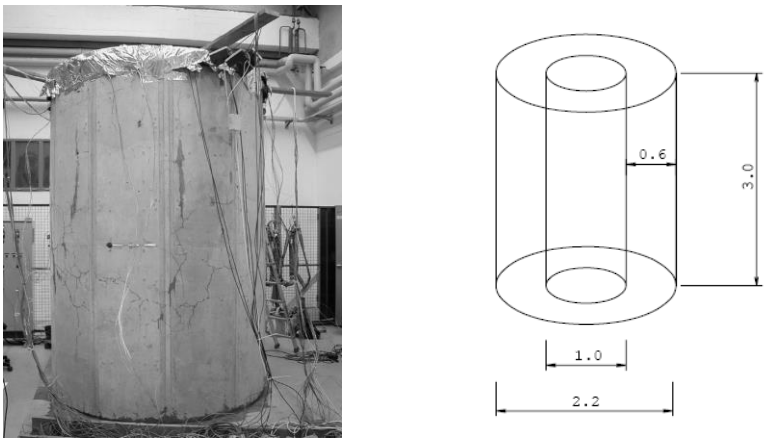

Figure 15. *Concrete hollow cylinder. Experimental device and geometry*

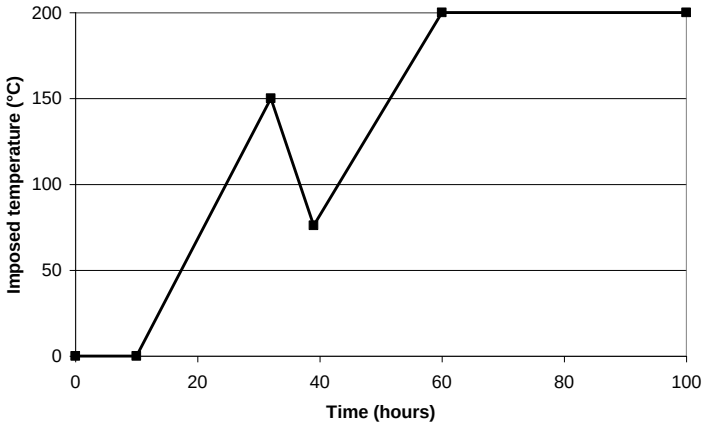

Figure 16. *Thermal loading*

For the calculation, a chained thermo mechanical approach has been chosen. The temperature distribution is computed first, using a linear thermal simulation. The boundary conditions consist in a zero flow on the top and bottom faces of the structure (thermally insulated condition). Convection and radiation are considered on the external face whereas the inner one is subjected to the imposed temperature (figure 17). The calculation is axisymmetric, with only a half structure modelled (vertical symmetry). Table 5 provides the material properties chosen for the thermal part of the simulation, and have been obtained from experiments (see Ranc et al, 2003 for more details). Figure 18 proposes a comparison between the computed temperatures and the experiment. Experiment and simulation are in a quite good agreement, especially on the outside surface but also in the inside of the volume even if some differences appear. Nevertheless, the thermal computation gives appropriate results. For the mechanical computation, only the thermal loading will be considered: it is indeed responsible for a thermal strain, using the expression provided in equation 3.

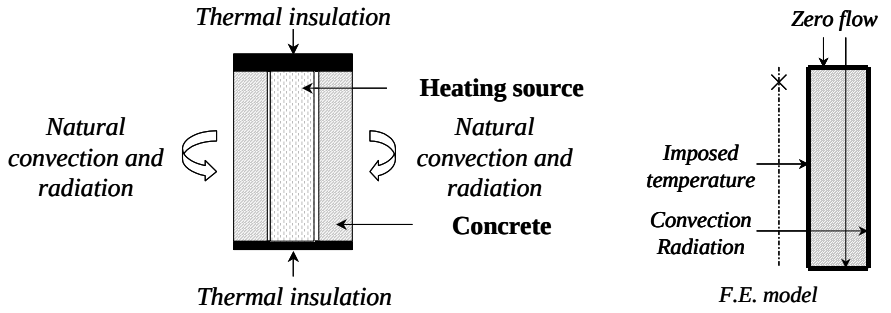

Figure 17. *Boundary conditions and loading for the hollow cylinder.*

Thermal conductivity ($W.m^{-1}.K^{-1}$)	2.3
Volumetric mass ($kg.m^{-3}$)	2370
Mass heat ($J.kg^{-1}.K^{-1}$)	1000
Emissivity	0.93
Convection coefficient ($W.m^{-2}.K^{-1}$)	5
Initial temperature (°C)	20

Table 5. *Coefficients for the thermal computation.*

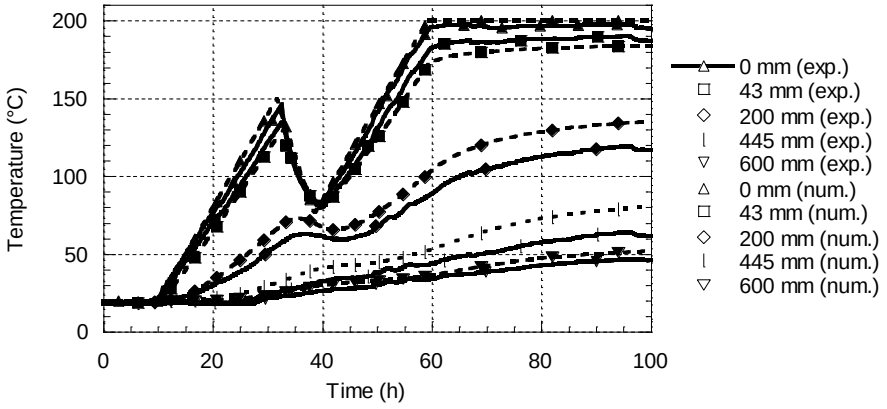

Figure 18. *Evolution of the temperature distribution in time inside the hollow concrete cylinder at different radial positions (from 0 mm (inside face) to 600 mm (outside face)) and comparison with the experiment.*

T (°C)	E (GPa)	σ_y (MPa)	f_c (MPa)	ε_m	ε_u
20	38.5	14	57	0.002	0.01
60	33	12	55	0.00021	0.0106
110	29.8	11	55	0.00023	0.015
250	20.4	8	46	0.00027	0.01608

Table 6. *Evolutions of the mechanical parameters with temperature for the plasticmodel. A linear evolution is supposed between the different temperatures.*

A zero vertical displacement is applied on the bottom line as boundary conditions (symmetry condition). Table 6 gives the material properties which are supposed to evolve with temperature (the temperature evolution is calibrated from experiments carried out in (Ranc et al, 2003)). As no information is provided concerning the tensile properties, they are kept constant (f_t = 4.8 MPa, G_f = 400 N/m), as well as the Poisson ration and the dilation coefficient (ν=0.2 and α_{th} =10^{-5} °C^{-1}). Steel reinforcement, that was not considered during the thermal computation for a seek of simplicity, is added for the mechanical part. It is composed with 25 mm diameter bars, except for the inner vertical bars with a 16 mm diameter (figure 19).

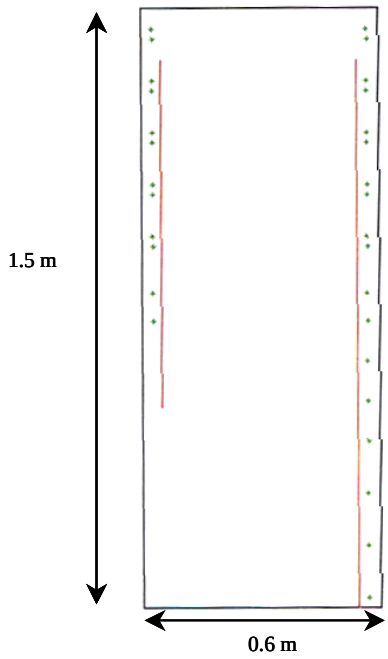

Figure 19. *Steel distribution in the reinforced concrete hollow cylinder for the finite element model.*

They are supposed elastic with E = 190 GPa, ν = 0.3, $\alpha_{th} = 10^{-5}$ °C^{-1}. Temperatures in the steel are defined from the preliminary thermal calculation using a projection from the concrete points.

Figure 20 illustrates the evolution of the radial and orthoradial strains on the inner face at mid height. The simulation is compared with some experimental results obtained from strain gauges. The model is globally able to reproduce the structural behaviour during loading (increase in the temperature). The vertical strains are correctly represented especially. For the orthoradial strains, an overestimation of the experimental results is observed. It could be explained by some simplifications in the simulation (position and / or modelling of the steel reinforcement and tensile parameters that are kept constant with temperatures). Moreover, hydrous phenomena (dehydration especially) are not taken into account in our simulation and would require some thermo – hydro – mechanical simulations that are not in the scope of the present study (Dal Pont et Ehrlacher, 2004). Nevertheless, the global behaviour is correctly simulated by the plastic constitutive law.

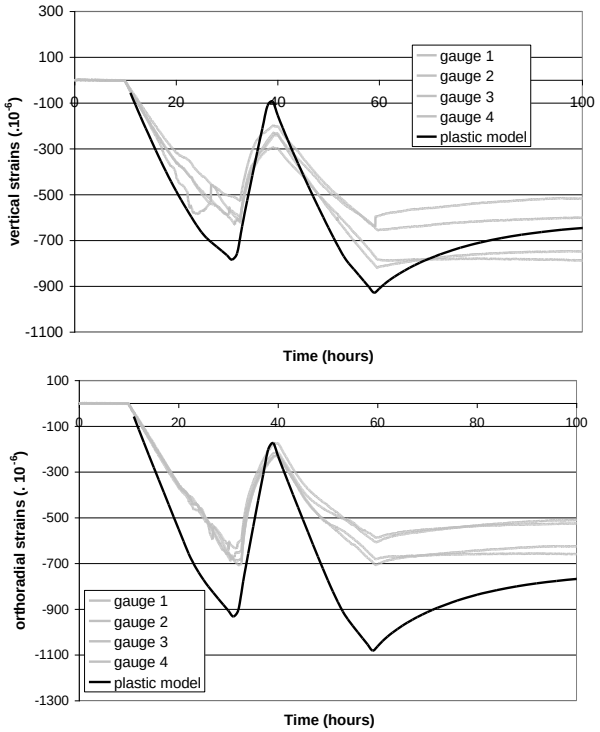

Figure 20. *Evolution of the vertical (on the top) and orthoradial strains at mid height on the inside face. Comparison between the simulation and the experiment*.

Figure 21 presents the tensile internal variable distributions at different loading steps. The mechanical degradation appears from the outside of the volume (cold face) then propagates to the center. As the structure is reinforced, characteristic localisation zones are observed that follow a crack pattern. At the end of the computation, a “crossing crack” is observed.

As a conclusion, the plastic model is able to reproduce qualitatively, for the evolution of the crack pattern, and quantitatively for the strains, the thermo – mechanical behaviour of the hollow concrete cylinder. Once again, one of the key point is the easiness to calibrate the material parameters from standard experimental tests and / or some default values.

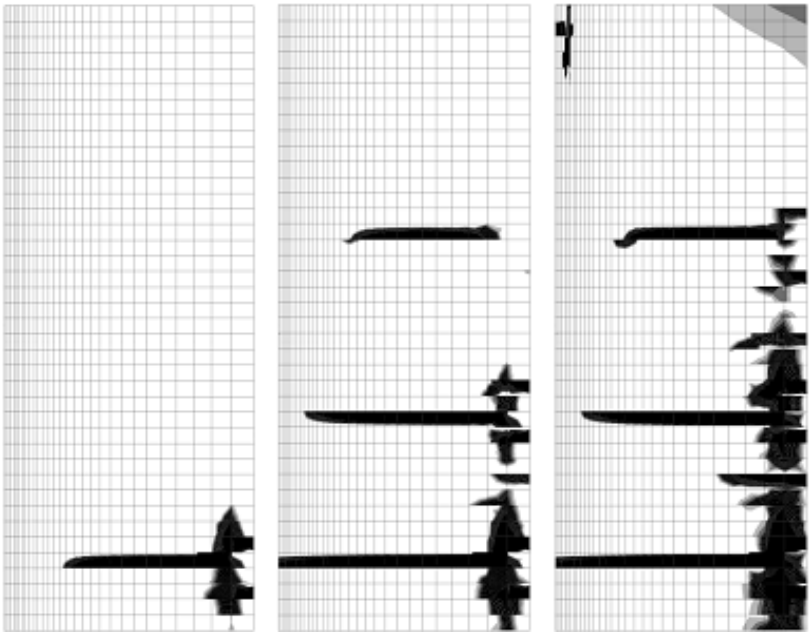

Figure 21. *Tensile internal variable distribution at different times. Black zones correspond to a heavy mechanical degradation*

5. Conclusions

An elastic plastic model for concrete has been presented. Based on two yield surfaces (one for tension and one for compression), it has been validated on both elementary and structural applications. For tension, the standard evolution is reproduced (elasticity then softening). For compression, the simulated monotonic behaviour is in agreement with experimental observations, both for the axial and volumetric measurements. Finally, the numerical strength envelopes in biaxial loading matches the experiment. For structural applications, it is shown that the proposed formulation is able to give appropriate results (beam or hollow cylinder), compared to other more complex formulations (benchmark on the three point bending beam)

Obviously, the constitutive law has its own limit. Some effects are not taken into account. Incorrect unloading is simulated and the choice for the plastic yield surface in compression is not adapted to represent the experimental evolutions for high confinement (decrease in the stiffness). Moreover, the plastic internal variables are not so relevant in particular cases (coupling between damage and permeability for

example). Nevertheless, in most encountered situations, the model is fully sufficient to provide a global view of the structural behaviour.

Except its relative simplicity, one of the key point of the formulation is the physical significance of the parameters. They can all be determined from standard tests (tension, compression) or more complex experiment (biaxial compression) for which default values are available. Moreover, they do not require the full stress – strain curve, as only characteristic points are needed (tensile strength, compressive strength). In an industrial context, where data are not always easily available, it represents a good compromise compared to other models that are also chosen for their simplicity but which do not seem so relevant to calibrate.

From this concept, keeping in mind the interest of "easy-to-calibrate" parameters, it could be interesting to improve the formulation, by modifying the yield surfaces or coupling the formulation with some damage law.

6. References

Cast3M, Description of the finite element code Cast3M, http://www-cast3m.cea.fr, 2006

Crouch R.S., Tahar B., "Application of a stress return algorithm for elasto plastic hardening softening models with high yield surface curvature", *Proceedings of European Congress on Computational Methods in Applied Sciences and Engineering (CD-ROM)*, Onate, E., et al (Eds), Barcelona, 2000

Dal Pont S., Ehrlacher A., "Numerical and experimental analysis of chemical dehydration, heat and mass transfers in a concrete hollow cylinder submitted to high temperatures", *International Journal of Heat and Mass Transfer*, 47, 2004, p. 135-147

Drucker D.C., Prager W., "Soil mechanics and plasticity analysis of limit design", *Quaterly journal of applied mechanics,* 10, 1952, p. 157-162

Feenstra P.H, de Borst R., "A composite plasticity model for concrete", *International Journal of Solids and Structures*, 33, 5, 1996, p.397-424

Ghavamian S., Delaplace A., "Modèles de fissuration de béton. Projet MECA", *Revue Française de Génie Civil*, 7, 5, 2003

Gopalaratnam V.S., Shah S.P., "Softening response of plain concrete in direct tension", *Journal of the American Concrete Institute,* May-June 1985, p. 310-323

Grassl P., Lundgren K., Gylltoft K., "Concrete in compression: a plasticity theory with a novel hardening law", *International Journal of solids and Structures*, 39, 2002, p. 5205-5223

Heinfling G., Contribution à la modélisation numérique du comportement du béton et des structures en béton armé sous sollicitations thermo-mécaniques à hautes températures, PhD Thesis, INSA Lyon, France

Jason L., Ghavamian S., Pijaudier-Cabot G., Huerta A., "Benchmarks for the validation of a non local damage model", *Revue Française de Génie Civil,* 8, 2004, p. 303-328

Jason L., Huerta A., Pijaudier-Cabot G., Ghavamian S., "An elastic plastic damage formulation for concrete : Application to elementary tests and comparison with an isotropic damage model", *Computational Methods in applied Mechanics and Engineering*, 195, 2006, p. 7077-7092

Kupfer H.B., Hilsdorf H.K., Ruesch H., "Behavior of concrete under biaxial stresses", *ACI Journal*, 66, 1969, p. 656-66

Kupfer H.B., Gerstle K.H., "Behavior of concrete under biaxial stresses", *Journal of engineering Mechanics*, 99, 1973, p.853-866

Lee S.K., song Y.C., Han S.H., "Biaxial behavior of plain concrete of nuclear containment buildings", *Nuclear Engineering and Design*, 227, 2004, p. 143-1453

Mazars J., Application de la mécanique de l'endommagement au comportement non linéaire et à la rupture du béton de structure, PhD Thesis, Université Paris VI, 1984

Menetrey P., Willam K. J., "Triaxial failure criterion for concrete and its generalization", *ACI Structural Journal*, 92, 3, 1995, p. 311-318

Millard A., Contribution à la modélisation à plusieurs échelles des matériaux et des structures, Dissertation, INSA de Lyon, 1996

Oller S., Onate E., Oliver J., Lubliner J., "Finite element nonlinear analysis of concrete structures using a plastic damage model", *Engineering Fracture Mechanics,* 35, 1990, p. 219-231

Ortiz M, Simo J.C., "An analysis of a new class of integration algorithms for elastoplastic constitutive relations", *International journal for numerical methods in engineering*, 23, 1986, p. 353-366

Picandet V., Khelidj A., Bastian G., "Effect of axial compressive damage on gas permeability of ordinary and high performance concrete", *Cement and Concrete Research*, 31, 2001, p. 1525-1532

Ranc G., Sercombe J., Rodrigues S., Gatabin C., "Structural and local behavior of reinforced high strength concrete structures subjected to high temperatures" *Proceeding of the fourth international conference on fracture mechanics of concrete and concrete structures*, Cachan, France, 2001

Ranc G., Sercombe J., Rodrigues S., "Comportement à haute température du béton de structure – Impact de la fissuration sur les transferts hydriques", *Revue Française de Génie Civil,* 7, 4, 2003, p. 397-424

Rots J.G., Computational modelling of concrete fracture, Dissertation, Delft University of Technology, the Netherlands, 1988

Simo J.C, Ju J.W., "Stress and strain based continuum damage models-I. Formulation", *International Journal of Solids and Structures,* 23, 1987a, p. 821-840

Simo J.C., Ju J.W., "Stress and strain based continuum damage models-II. Computational aspects" , *International Journal of Solids and Structures,* 23, 1987b, p. 841-869

Sinha B.P., Gerstle K.H., Tulin L.G., "Stress-strain relations for concrete under cyclic loading", *Journal of the American Concrete Institute*, Februray 1964, p. 195-211

Sfer D., Carol I., Gettu R., Etse G., “Study of the behaviour of concrete under triaxial compression”, *Journal of Engineering Mechanics,* 128, 2, 2002, p. 156-163

Sugiyama T., Bremmer T.W., Tsuji Y., “Determination of chloride diffusion coefficient and gas permeability of concrete and their relationship”, *Cement and Concrete Research*, 26, 5, 1996, p. 781-790

Tailhan J-L., Colina H., Clément J-L., « Tests d’évaluation de modèles de comportement non linéaires pour le béton fissuré », *Revue Française de Génie Civil*, 7, 2003, p.691-707.

Ulm F-J., “Un modèle d’endommagement plastique: application aux bétons de structure”*Etudes et Recherches des laboratoires des ponts et chaussées*, Série ouvrages d’art, OA19, 1996

Yazdani S., Schreyer H.L., “Combined plasticity and damage mechanics model for plain concrete”, *Journal of Engineering Mechanics,* 116, 1990, p. 1435-1450